FIELD MAPPING AND CORRECTIONS OF THE MAGNET OF A RADIO-FREQUENCY MASS SPECTROMETER *

A. Coc, R. Fergeau, M. Jacotin, J.F. Képinski, R. Le Gac, G. Le Scornet,
M. de Saint Simon, C. Thibault, F. Touchard
CSNSM-IN2P3-CNRS, Bât 108, F-91405 Orsay-Campus

R. Grabit, G. Petrucci, G. Stefanini
CERN, CH-1211 Genève

1990

Abstract

The design of the magnet for a radio-frequency mass spectrometer with resolving power in the range 10^5 to 10^6 is presented. The required homogeneity and initial physical characteristics of the magnet are summarized. Then, the experimental methods which have been used for field mapping and field corrections are explained. Final performances of the magnet homogeneity are given, which already provide a resolving power of 3×10^5, in agreement with the original goal.

1 Introduction

A Radio-Frequency Mass Spectrometer -RFMS- based on the same principles as the one proposed and carried out by L.G. Smith[1, 2] has been built in order to be able to measure masses with a high accuracy. The main advantages of RFMS as compared to classical mass spectrometers, are that higher resolving powers are effectively reached, and moreover, that masses are compared through frequency measurements instead of voltage measurements. The present utilization of the RFMS that we built aims to determine the proton-antiproton mass ratio with an accuracy in the range of 10^{-9} (PS189 experiment at CERN).

The principle of the method of mass measurements using a RFMS has already been given [3, 4, 5]. Let us recall briefly the main points : the mass of the particle of interest is obtained from the measurement of its cyclotron frequency ω_c in an homogenous magnetic field B_0, using the relation : $\omega_c = qB_0/M$, where M is the mass of the particle and q its electric charge. The magnetic field is calibrated by using a reference particle whose mass is known. In the case of the proton-antiproton mass ratio, H^- ions are used for this purpose.

Particles are injected in the magnetic field following an helicoidal trajectory of radius R_0 and of dip angle λ_0. They make two turns in the field before being ejected. At the first half turn and at one turn and half, a RF modulation is applied to the particle, therefore modifying its energy. Because of trajectory defining slits at the inlet and outlet of the magnet, only those particles whose total energy is unchanged will be ejected. It can be easily shown that the total modulation of the energy of a given particle is zero when the frequency ω of the modulation fulfills the condition : $\omega = (n + 1/2)\omega_c$ with n integer. The transmission of the spectrometer is scanned as a function of the frequency of the modulation, and peaks of maximum transmission are observed when the resonance condition is

*Nucl. Instr. and Meth. **A305** (1991) 143–149

matched.
The theoretical resolving power of such a spectrometer has been given in a previous paper [6]. Assuming a perfect isochronism of trajectories and an ideal RF modulator, it has been calculated to be 10^6 in our case. In next chapter, we shall give the corresponding required homogeneity criteria. In chapter 3, we shall present the design of the magnet and the different shimmings used to correct and control the field. In chapter 4, we shall describe the measurement set-up. Finally, in chapter 5 we shall comment the obtained performances.

2 Homogeneity criteria

Due to the principle of the spectrometer, the modulation splits the trajectories of the particles. Furthermore, the particles may enter the magnetic field at different positions and angles compatible with the slits dimensions. Consequently, inhomogeneities in the magnetic field will lead to unwanted variations in the transit time and trajectories of the particles.
Quantitatively, the variation δR of the position of the trajectories should not exceed half the width ($w/2 = 0.1$mm) of the modulator slits and the relative change in the transit time should be negligible when compared to the relative width of a RF peak, *i.e.* the cyclotron frequency variation $\delta\omega_c/\omega_c$ should be smaller than the inverse of the resolving power. .

2.1 Magnetic field parametrization

The general design of the magnet and the coordinate system (R, ϕ, z) which has been used for field mapping are shown in Fig. 1.

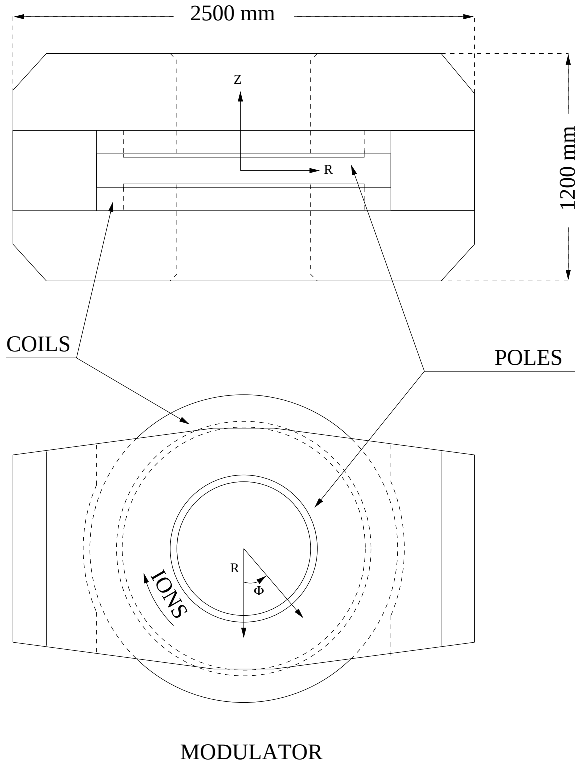

Figure 1: General magnet layout

Between the two modulations, the ideal helicoidal mean trajectory is defined by $R = R_0$, and $z = z_0(\phi)$.

It is followed by the ions according to decreasing ϕ and z, from $\phi = 2\pi,\ z_0(2\pi) = z_1 = 15$ mm down to $\phi = 0,\ z_0(0) = -z_1$, so that $z_0(\phi) = -z_1 + R_0\phi \tan\lambda_0$ where λ_0 is the dip angle of the helicoidal mean trajectory ($2\pi R_0 \tan\lambda_0 = 2z_1$). In the vicinity of the mean trajectory, the field main component can be written :

$$B_z(R,\phi,z) = B_z(R_0,\phi,z_0(\phi)) + (R-R_0)\left[\frac{\partial B_z}{\partial R}\right]_{(R_0,\phi,z_0(\phi))} + (z-z_0(\phi))\left[\frac{\partial B_z}{\partial z}\right]_{(R_0,\phi,z_0(\phi))} \qquad (1)$$

where the coefficients of the development depend only on ϕ once the parameters defining the mean trajectory have been fixed. They are more conveniently expressed as Fourier's series. Using the mean field value B_{0z} as normalization factor, we may define the following Fourier coefficients :

$$\frac{B_z(R_0,\phi,z_0(\phi)) - B_{0z}}{B_0 z} = \sum_{n=1}^{\infty}[a_n(R_0,\lambda_0)\cos(n\phi) + b_n(R_0,\lambda_0)\sin(n\phi)] \qquad (2)$$

$$\frac{1}{B_{0z}}\left[\frac{\partial B_z}{\partial R}\right]_{(R_0,\phi,z_0(\phi))} = a_{0,R}(R_0,\lambda_0) + \sum_{n=1}^{\infty}[a_{n,R}(R_0,\lambda_0)\cos n\phi + b_{n,R}(R_0,\lambda_0)\sin n\phi]\ \mathrm{cm}^{-1} \qquad (3)$$

And a similar expression for $(1/B_{0z})(\partial B_z/\partial z)$.
The various Fourier coefficients $a_n, b_n, a_{n,R},\ b_{n,R},\ a_{n,z},\ b_{n,z}$ describe the field inhomogeneities.

2.2 Limits on the inhomogeneities

The calculation of the effect of small inhomogeneities on the motion of particles in a magnetic field is rather long [7] and will not be described here : the differential equation of the motion is tranformed into an integral equation, after which the integration is performed along the ideal trajectory using the Fourier coefficients to parametrize the magnetic field. As already mentioned, when the parameters defining the trajectory span the acceptance, the requirements are that $\delta R \ll w/2$ to hold the transmission at its maximum and $\delta\omega_c/\omega_c \ll 10^{-6}$ to hold the resolving power at 10^6.
A first conclusion from these calculations is that only the very low order Fourier coefficients with $n \leqslant 2$ need to be considered.
Second, the limitations for these coefficients are obtained. Concerning the radial displacement δR, the limitation is $(a_n, b_n) < w/2\pi R_0$, which leads to $(a_n, b_n) < 10^{-4}$. Concerning the isochronism, the limitations then deduced from calculations [7] are also $(a_n, b_n) < 10^{-4}$ for the main component. For the gradients, they are $(b_{n,R}, a_{n,z}, b_{n,z}) < 2 \times 10^{-6}\mathrm{cm}^{-1}$.
A further result from calculations [7] is that in order to compensate for relativistic effects generated by the modulation of the energy around 200 keV, the combination $a_R = (3a_{0,R}/2 - a_{1,R} + a_{2,R}/4)$ should be tuned at $4.2 \times 10^{-6}\mathrm{cm}^{-1}$, which can be obtained by tuning the radial gradient uniformly to

$$\frac{1}{B_0 z}\frac{\partial B_z}{\partial R} \simeq 2.8 \times 10^{-6}\mathrm{cm}^{-1}$$

with $(a_{1,R},\ a_{2,R}) < 10^{-6}\mathrm{cm}^{-1}$.

3 Magnet design

3.1 Magnet

The main characteristics of the magnet are given in Table 1.
The yoke and the poles are made of low carbon steel. The pole piece profile is flat. A first attempt towards homogeneity was made through the mechanical quality of the pole surfaces, a precisely calibrated gap height, and 10 mm Purcell gaps between the yoke and the pole pieces. Homogeneity along

Total weight	22 tons
Pole piece inner diameter	660 mm
Pole piece outer diameter	1340 mm
Pole piece thickness	130 mm
Main gap height	140 mm
Purcell gaps height	10 mm
Field range	0.1–0.8 T
Designed field for PS189	0.13 T
Main coil	5 pancakes 22 turns each coil
Main coil resistance	0.28 Ω
Main coil inductance	0.45 H
Main coil time constant	≈1.6 s
Power at 0.13 T	1.6 kW

Table 1: Magnet parameters

the radial direction has been enhanced by using magnetic ARMCO iron shims along the inner and outer circumferences of the pole pieces. The thickness of the shims has been experimentally determined. The adopted values (1.5 mm and 2.0 mm respectively) are in good agreement with the ones computed by the CERN program package POISCR.

3.2 Pole face correction printed circuits

The correction of azimuthal inhomogeneities and the control of the radial and axial gradients are achieved by using pole face coils. A general discussion of the electrical current shims can be found in ref.[8]. The designs of the printed circuits corresponding to the different coils (Fig. 2) are such that each set of loops acts on 1 only of the 3 parameters B_z, $\partial B_z/\partial R$ and $\partial B_z/\partial z$ without affecting the two others. There are 8 groups of such coils on each pole piece, therefore enabling corrections up to n=2 terms in Fourier developments.
Assuming that the pole pieces are infinite, the efficiencies of these loops may be calculated by the image method as used by Neyret and Parain [9]. Using a computer, an exact calculation may be performed [10]. However, if the loops are approximated by considering 2 infinite parallel wires instead of the azimuthal finite ones, thus neglecting the radial wires, it is possible to get analytic formulae [10] much easier to use. Even in our case where the loops are not very much stretched, it has been shown [10] that the accuracy of these formulae, as compared to the computed values, is better than 10^{-3} for b_z, and of the order of a few percent for $\partial b_z/\partial R$ and $\partial b_z/\partial z$. The assumption that the pole pieces are infinite is estimated to result in a few percent differences for all values.
Defining $2h$ as the main gap height and $2l$ as the radial extension of the loop, the efficiencies in the center of an octant are found to be :

- $$\frac{b_z}{I} = \frac{\mu_0}{h} \tanh \frac{\pi l}{2h} \qquad (4)$$

For $h = 0.07$ m and $l = 0.115$ m (Fig. 2a), one gets :
$b_z/I = 0.18 \times 10^{-4}$ T A^{-1} = 0.18 G A^{-1}.

- $$\frac{1}{I}\frac{\partial b_z}{\partial R} = \frac{\mu_0}{hp} \tanh \frac{\pi l}{2h} \qquad (5)$$

where p is the distance between 2 successive wires (Fig. 2b). In this formula, the negative effect of the loop-closing wires has been neglected. In our case, their effect is 4×10^{-2}. However a more complete

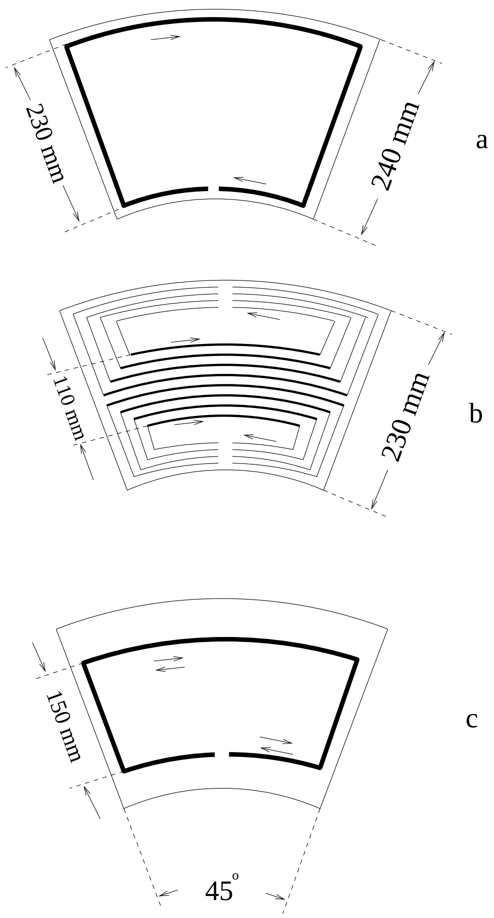

Figure 2: Pole face printed circuits used for electrical current shimming : (a) main component; (b) radial gradient; (c) axial gradient.

formula may take them into account[10].
For $h = 0.07$ m, $l = 0.055$ m, and $p = 2l/7 = 0.11/7$, one gets :
$(1/I)(\partial b_z/\partial R) = 9.6 \times 10^{-4}$ T m^{-1} A^{-1} = .096 G cm^{-1} A^{-1}.

- $$\frac{1}{I}\frac{\partial b_z}{\partial z} = \frac{\pi\mu_0}{2h^2}\frac{\sinh\frac{\pi l}{2h}}{\cosh^2\frac{\pi l}{2h}} \tag{6}$$

For $h = 0.07$ m and $l = 0.075$ m (Fig. 2c), one gets :
$(1/I)(\partial b_z/\partial z) = 1.4 \times 10^{-4}$ T m^{-1}A^{-1} = 0.014 G A^{-1}cm^{-1}.
The currents in the loops are established with 12 bits DACs in a CAMAC computer driven system so that the Fourier coefficients can be adjusted with an accuracy of 10^{-6} for the main component, 2×10^{-7} cm^{-1} for the radial gradient, and 2×10^{-8} cm^{-1} for the axial gradient. The efficiencies measured in the center of each octant were found to be respectively 0.17 G A^{-1}, 0.095 G cm^{-1} A^{-1}, and 0.013 G cm^{-1} A^{-1}, in very good agreement with the calculated ones.

4 Experimental method for magnetic field measurements

The quantities to be measured to check the qualities of the magnet are :
- the field components B_z, B_R, B_ϕ as functions of ϕ at differents values of the radius and of the

height in the gap;

- the gradient $\partial B_z/\partial R$ as a function of ϕ at different heights;
- the gradient $\partial B_z/\partial z$ as a function of ϕ at different radii.

4.1 Field mapping

A device composed of four Hall probes mounted on a movable gear has been built to determine the intensities B_R, B_ϕ, B_z in directions R, ϕ, z of the magnetic field. The probes are fixed on a non metallic stiff bar as shown on Fig. 3. The gear can move in the 3 directions R, ϕ and z. The position of the device and axes of motion have been set very accurately relatively to the magnet. Computer driven stepping motors ensure the displacements by steps of $\delta\phi \approx 1$ mrad and $\delta R = \delta z \approx 0.05$ mm. The sensivity of the Hall probes is $K \approx 14\,\mu$V G^{-1}. The B_z probes are calibrated with a NMR magnetometer. No dynamical temperature stabilization is performed. However, temperature is monitored by a transducer on the probe with an accuracy $\delta T \approx 0.1^0$C.

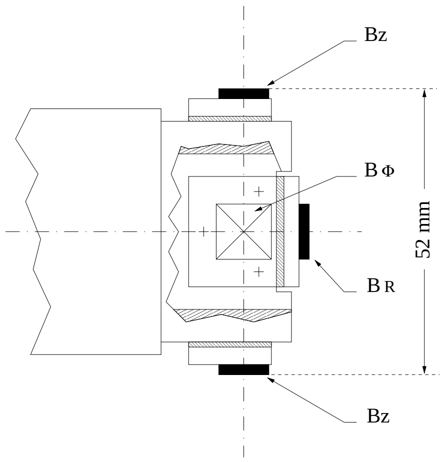

Figure 3: Arrangement of the Hall probes for field mapping

The Hall probes give only relative variations of the B_R and B_ϕ components. Absolute values of B_R have been obtained with a Hall probe pendulum similar to the induction flip coils. The B_ϕ component has no influence on the particle trajectory and is no longer considered.

4.2 Gradient measurements

For a given value of ϕ, the radial and axial gradients are determined with the movable gear : the main component of the field is measured six times over a given distance (60 mm for the radial gradient, and 50 mm for the axial one). A linear fit is then performed to extract the value of the gradients. The accuracy is of the order of 10^{-2} G cm^{-1}, *i.e.* 10^{-5} cm^{-1} at the designed field $B_z = 1300$ G.
A very accurate, but rather heavy to handle, method has also been used for the radial gradient. A 0.8 Hz oscillating radial motion of some millimeters of amplitude is given to the Hall probes. The frequency and the amplitude of the movement are set very precisely by a synthetiser and a step counter. The oscillation of the probe in the non-uniform field generates a signal whose Fourier components are analysed by a spectrum analyser. The sentivity reaches 10^{-3} G cm^{-1}. Both methods have been compared and were found in agreement.

4.3 Normalisation procedures

Hall probes are very sensitive to the environment. In particular, their temperature and their driving currents must be carefully controlled during the measurement. The magnet power supply is also rather sensitive to the ambient temperature. The value of the current is therefore measured with an accurate shunt. All these factors have been steadily studied and adequate corrections were applied to the results. A good check is achieved when the value of B_z at the beginning and at the end of a 2π azimuthal scan is indeed the same. An "absolute" value of the field is obtained using a NMR magnetometer.

5 Results

Measurements have been performed inside different planes parallel to the pole pieces :

- B_z versus ϕ at $z=$ 25 and -27 mm (Fig. 4)
- $\partial B_z/\partial R$ versus ϕ at $z=$ 25, 0, -27 mm (Fig. 5)
- $\partial B_z/\partial z$ versus ϕ at R=500 mm (Fig. 6)

Experimental Fourier coefficients were first determined in these planes. They allowed to perform a linear interpolation of B_z and of $\partial B_z/\partial R$ along the helicoidal mean trajectory (Figs. 5 and 6). Final Fourier coefficients were then extracted to be compared to the required values. They are reported in Table 2 and Table 3.

5.1 Magnet without electrical current shims

In Table 2, are given the values of Fourier coefficients obtained after magnetic shimming only. The

	0	1	2	3
Main component				
a	-	3.9×10^{-5}	$-27. \times 10^{-5}$	-0.08×10^{-5}
b	-	2.9×10^{-5}	-2.2×10^{-5}	-3.9×10^{-5}
Radial gradient [cm^{-1}]				
a	$42. \times 10^{-6}$	8.6×10^{-6}	-5.4×10^{-6}	-1.7×10^{-6}
b	-	0.7×10^{-6}	4.7×10^{-6}	3.3×10^{-6}
Axial gradient [cm^{-1}]				
a	$-21. \times 10^{-6}$	-0.66×10^{-6}	-5.0×10^{-6}	-0.17×10^{-6}
b	-	-7.2×10^{-6}	-7.1×10^{-6}	-1.1×10^{-6}

Table 2: Fourier coefficients on the mean trajectory without electrical shims

very prominent feature of $B_z(\phi)$ is the presence of an azimuthal modulation, with bumps roughly centered at $\phi = \pi/2$ and $3\pi/2$, corresponding to the yoke return blocks (Figs. 1 and 4).
The harmonic term b_1 is associated to a residual wedge deformation of the main gap. It could be mechanically suppressed. However, a more flexible and reliable compensation is achieved by using electrical current shims, as it will be seen below.
The higher order terms describe the field bumps. This modulation is naturally due to the different pathes of the flux lines in the two main symmetry planes of the magnet. The amplitudes of the two bumps are not identical, very likely because of local differences across the yoke intermediate blocks contact surface, where the flux density varies rapidly.
The gradients of the main component in the useful gap are found to be :

$$\frac{1}{B_{0z}}\frac{\partial B_z}{\partial R} \simeq 4 \times 10^{-5}\mathrm{cm}^{-1}, \quad \text{and} \quad \frac{1}{B_{0z}}\frac{\partial B_z}{\partial z} \simeq -2 \times 10^{-5}\mathrm{cm}^{-1}$$

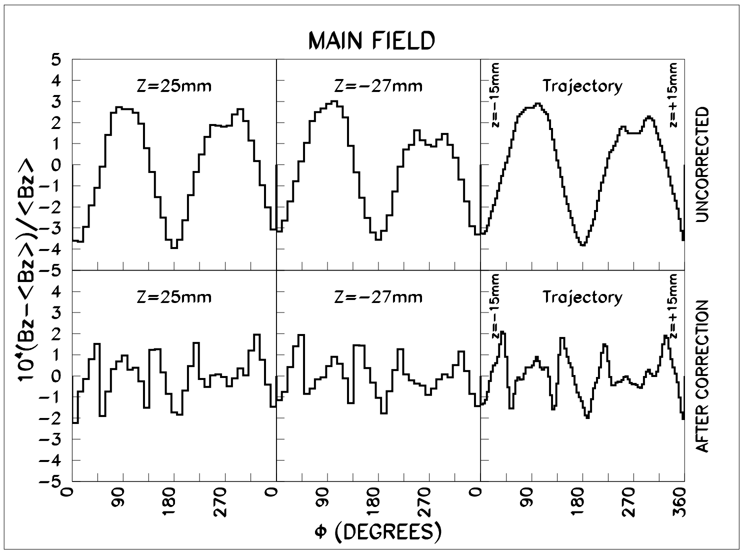

Figure 4: Measured main component $(B_z - B_{0z})/B_{0z}$ and interpolated value along the mean trajectory

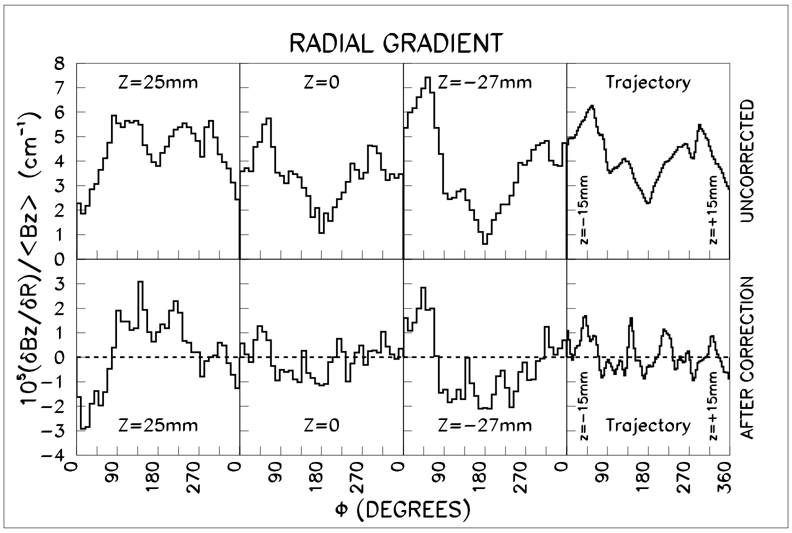

Figure 5: Measured radial gradient $(1/B_{0z})(\partial B_z/\partial R)$ and interpolated value along the mean trajectory

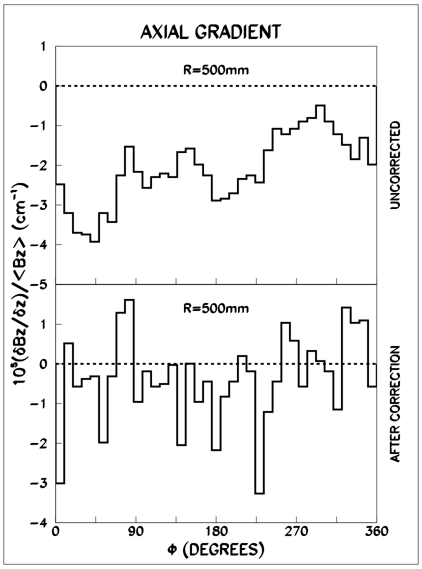

Figure 6: Measured axial gradient $(1/B_{0z})(\partial B_z/\partial z)$

which is rather independent of the azimuth.
The B_R component has been measured with the Hall pendulum. Before magnetic shimming, one finds : $B_R/B_{0z} \simeq 1 \times 10^{-4} + 2 \times 10^{-4} \sin\phi \quad (z = 0,\ R = R_0)$. The offset average amplitude is certainly due to a residual conicity of the pole pieces. The azimuthal modulation exhibits the same periodicity as B_z and has probably the same origin. After magnetic shimming, the radial component of the field B_R is reduced to the limit of the sensivity of the Hall pendulum, namely : $B_R/B_{0z} \simeq 3 \times 10^{-5} \quad (z = 0,\ R = R_0)$ and this at both $\phi = 0$ and $\pi/2$.

5.2 Magnet corrected by electrical current shims

In Table 3, are given the final values of Fourier coefficients obtained after adjusting the electrical currents in the loops in order to minimize them. a_n and b_n are found to be well below 10^{-4}. For

	0	1	2	3
Main component				
a	-	1.5×10^{-5}	-1.5×10^{-5}	0.55×10^{-5}
b	-	0.3×10^{-5}	-1.7×10^{-5}	-1.1×10^{-5}
Radial gradient [cm^{-1}]				
a	0.97×10^{-6}	1.6×10^{-6}	1.8×10^{-6}	0.06×10^{-6}
b	-	0.53×10^{-6}	2.9×10^{-6}	0.91×10^{-6}
Axial gradient [cm^{-1}]				
a	-3.7×10^{-6}	4.1×10^{-6}	-3.1×10^{-6}	-1.5×10^{-6}
b	-	-0.46×10^{-6}	-2.1×10^{-6}	-2.1×10^{-6}

Table 3: Fourier coefficients on the mean trajectory with electrical shims

the gradients, taking into account the fact that the accuracy of measurements is of the same order of magnitude as the required values, $a_{n,R}$, $b_{n,R}$, $a_{n,z}$, $b_{n,z}$ are satisfying too, but they will have to be adjusted more precisely by looking at the performances of the spectrometer itself.
The residual azimuthal modulation of the radial gradient (Fig. 5) cannot be completely cancelled because it is antisymmetrical relative to the middle plane z=0. It is probably due to a misalignment of the centres of the pole pieces.

5.3 Field stability

Unwanted field changes can originate from many different sources : mechanical deformations due to temperature variations, eddy currents, fluctuations of the main dc power supply, etc...
Temperature variations are smoothed by the thermal capacitance of the yoke.
Eddy currents can bring troubles concerning the reproducibility of the field. A demagnetization cycle and very slow variations when modifying the settings of the field have proved to give consistently the same field pattern, within the measuring resolution.
The stray conductance to ground of the cooling circuit has been drastically reduced by using a closed circuit freon cooling system.
The fluctuations due to the main coil current noise have been investigated carefully. "High" frequency fluctuations (above 1 Hz) are strongly suppressed. The low frequency spectrum of the field fluctuations has been studied by Fourier analysis of the signal from the NMR probe. Below 0.5 Hz, unstabilities of the field are mainly due to current variations of the main dc power supply. They are presently found to be less than the limit of the NMR resolution ($\approx 10^{-6}$).

6 Conclusions

Using both magnetic and electric shimming, we indeed succeeded to satisfy the required homogeneity criteria. Varying the currents in electrical shims, both radial and axial gradients may be controlled and accurately adjusted. As shown, a first adjustment could be performed which minimizes the experimental Fourier coefficients within the limit of sensitivity of field mapping.
However the transmission and resolving power of the RFMS are more sensitive to gradient values than the measuring system, so that the ultimate adjustment must be achieved by checking it through the optimization of the performances of the RF Mass Spectrometer. Such a fine tuning could be performed by using the H^- ion source built for the proton-antiproton mass comparison. Presently, the transmission inside the magnet agrees reasonably well with the expected one, and a resolving power of 3×10^5 is currently obtained, very near the value of 5×10^5 given by simulations taking into account the real dimensions of the modulator.

References

[1] L.G. Smith, Proc. Int. Conf. on Nuclidic Masses, ed. H. E. Duckworth (Univ. of Toronto Press, Toronto, Canada, 1960) p.418.

[2] L.G. Smith, Proc. 3rd Int. Conf. on Atomic Masses, ed. R. C. Barber (Univ. of Manitoba Press, Winnipeg, Canada, 1967) p.811.

[3] G. Audi, A. Coc, M. Epherre, R. Fergeau, P. Guimbal, M. de Saint Simon, C. Thibault, F. Touchard, E. Haebel, H. Herr, R. Klapisch, G. Lebée, G. Petrucci and G. Stefanini, Proposal CERN PSCC/81-84 (1981).

[4] A. Coc, R. Fergeau, C. Thibault, M. de Saint Simon, F. Touchard, E. Haebel, H. Herr, R. Klapisch, G. Lebée, G. Petrucci and G. Stefanini, Int. Rept. LRB 85-01, CSNSM, Orsay (1985).

[5] A. Coc, R. Fergeau, C. Thibault, M. de Saint Simon, F. Touchard, E. Haebel, H. Herr, R. Klapisch, G. Lebée, G. Petrucci and G. Stefanini, Proc. 3rd LEAR Workshop, ed. U. Gastaldi, R. Klapisch, J.M. Richard and J. Tran Thanh Van (Ed. Frontières, Gif sur Yvette, France, 1985) p.675

[6] A. Coc, R. Le Gac, M. de Saint Simon, C. Thibault and F. Touchard, Nucl. Instr. and Meth. **A271** (1988) 512.

[7] A. Coc, PS189/CERN/88-01 and 89-01 Notes.

[8] W.A. Anderson, Rev. Sci. Instr. **32** (1961) 241.

[9] G. Neyret and J. Parain, Nucl. Instr. and Meth. **5** (1959) 259.

[10] C. Thibault, PS189/CERN/90-02 Note (1990).